

# Measurement of the Bidirectional Reflectance Distribution Function of Tungsten Surface Sputtered in Argon Plasma<sup>\*)</sup>

Hiroki NATSUME, Kunpei NOJIRI<sup>1)</sup>, Shin KAJITA<sup>2)</sup>, Tomohiko USHIKI<sup>1)</sup>, Tatsuo SUGIE<sup>3)</sup>, Sin-iti KITAZAWA<sup>1)</sup>, Takanori KIKUCHI<sup>1)</sup>, Tomohiro YOKOZUKA<sup>1)</sup>, Hirohiko TANAKA, Noriyasu OHNO and Takaki HATAE<sup>1)</sup>

*Graduate School of Engineering, Nagoya University, Nagoya 464-8603, Japan*

<sup>1)</sup>*Naka Fusion Institute, National Institutes for Quantum Science and Technology (QST), Naka 311-0193, Japan*

<sup>2)</sup>*Institute of Materials and Systems for Sustainability, Nagoya University, Nagoya 464-8603, Japan*

<sup>3)</sup>*Nippon Advanced Technology Co., Ltd., Tokai, Naka District 319-1112, Japan*

(Received 23 December 2021 / Accepted 10 March 2022)

For ITER spectroscopic measurements, it is important to understand the optical reflection characteristics of the divertor surface for an accurate measurement because the stray light in the divertor may be large. We set up a goniophotometer that measures the optical reflection characteristics and investigated the bidirectional reflectance distribution function of tungsten samples sputtered in an argon plasma. The specimens sputtered at temperatures lower than the recrystallization temperature of tungsten exhibited smooth surfaces and strong specular reflections in their optical reflectance characteristics. Recrystallized crystals likely grew for the specimens sputtered at temperatures approximately equal to the recrystallization temperature, resulting in a weak specular reflection.

© 2022 The Japan Society of Plasma Science and Nuclear Fusion Research

Keywords: bidirectional reflectance distribution function, goniophotometer, sputtering, spectroscopic diagnostics

DOI: 10.1585/pfr.17.2405041

## 1. Introduction

Stray light is a significant issue in spectroscopic diagnostics. The ITER divertor is made of tungsten, which has high optical reflectance; hence, the accuracy of a spectroscopic measurement is at the risk of degradation, as the measured signal may be affected by the reflected light from the divertor region [1]. Therefore, it is crucial to consider the effects of reflection on the accuracy of measurements.

Recently, a ray-tracing approach that allows the quantitative evaluation of the effects of reflected light has been studied and developed [2]; combined with tomography techniques, it enables the removal of stray light [3,4]. This approach has been applied to spectroscopic diagnostics in ITER, including  $H_\alpha$  spectroscopy diagnostics [4] and divertor impurity monitoring [3,5]. The performance of the quantitative evaluation and removal of reflected light depends on the accuracy of optical reflection modeling. As in [6–8], the optical reflection characteristics of samples with machine marks have been studied. Considering the optical reflection characteristics of plasma-facing components and because the surface condition varies by plasma-wall interactions [9,10], the optical reflection characteristics also change depending on the condition of the divertor surface. However, the relationship between the optical reflection characteristics and a surface irradiated by plasma

has not yet been investigated in detail, although determining this relationship is necessary to realize accurate reflection modeling.

In this study, we first constructed a goniophotometer that measured the optical reflection characteristics corresponding to the surface condition of a sample. Additionally, we investigated the bidirectional reflectance distribution function (BRDF) of tungsten samples sputtered with various incident ion energies in an argon plasma.

The remainder of this paper is organized as follows. In Section 2, BRDF measurement using a goniophotometer is described. In Section 3, the sputtering experiment and sputtered samples are explained. The results and discussions of the BRDF measurements are presented in Sections 4 and 5, respectively. Finally, a summary is presented in Section 6.

## 2. BRDF Measurements

A schematic of the reflected light measurement and a picture of the goniophotometer are shown in Fig. 1, where subscripts “i” and “r” denote the incident and reflected quantities, respectively. The laser beam from the laser diode was incident on the specimen. The power of the reflected light from the specimen surface ( $P_r$ ) was measured using a light power meter (THORLABS, Inc.: S120VC, PW400) while changing its position using a motor via a belt pulley. The diameter and wavelength of the laser beam ( $\lambda$ ) were 1.2 mm and 473 nm, respectively. The wavelength

author's e-mail: natsume.hiroki@d.mbox.nagoya-u.ac.jp

<sup>\*)</sup> This article is based on the presentation at the 30th International Toki Conference on Plasma and Fusion Research (ITC30).

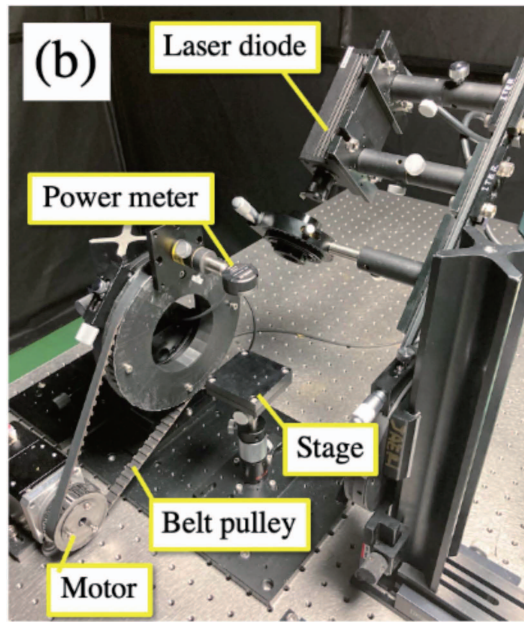
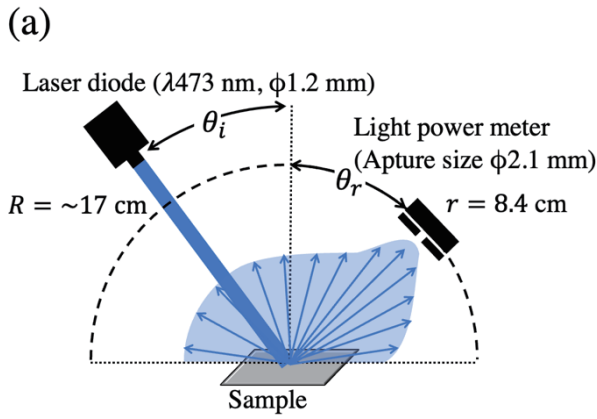


Fig. 1 (a) Schematic of the measurement system and (b) picture of the goniophotometer.

of the laser beam was almost equal to that of the  $H\beta$  emission (486 nm). In addition, the laser beam was linearly polarized with a vertical polarization of less than 0.1%. In the case of metals, the incident light can stimulate the motion of electrons near the surface, which in turn leads to the reflection of a wave, and there is quite little penetration in the depth direction [11]. Consequently, reflections from the metal occur at the surface [12]. Therefore, we regarded the reflected light as having no internal reflections that did not contribute to the diffusion component.

The BRDF is the ratio of the radiance of the reflected light to the irradiance of the incident light. Using the measured  $P_r$  and incident beam power ( $P_i$ ), the BRDF can be expressed as follows:

$$BRDF = \frac{P_r}{P_i \cos \theta_r \Omega_r}, \quad (1)$$

where  $\Omega_r$  denotes the solid angle projected onto the light-power meter. The  $P_r$  obtained at a specific reflection angle includes the power of light reflected at other reflection

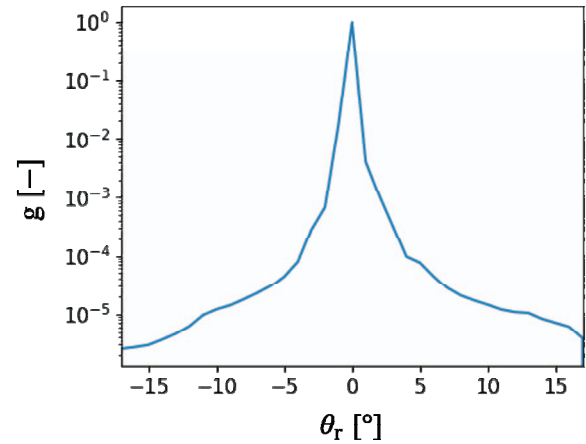


Fig. 2 Device function  $g(\theta_r)$ .

angles; hence, the size of the laser beam is finite. Mathematically, the measured reflected light power ( $P_{r,measure}$ ) could be regarded as the convolution integral of the pure reflected light power ( $P_{r,pure}$ ) with a device function ( $g$ ) that expresses the spread of the laser beam as follows:

$$P_{r,measure}(\theta_r) = \sum_{k=\theta^-}^{\theta^+} P_{r,pure}(k)g(\theta_r - k). \quad (2)$$

To obtain  $P_{r,pure}$ , we performed deconvolution to  $P_{r,measure}$  as follows:

$$P_{r,pure} = \mathcal{F}^{-1}[\mathcal{F}[P_{r,measure}]/\mathcal{F}[g]], \quad (3)$$

where  $\mathcal{F}[\cdot]$  represents the discrete Fourier transform and  $\mathcal{F}^{-1}[\cdot]$  is the inverse discrete Fourier transform. The device function was determined by normalizing the integrated value to unity for the measured reflected light from the aluminum mirror, as shown in Fig. 2. All the measured reflected powers in this study were decomposed.

### 3. Sputtering Experiment

Figure 3 shows a schematic of the experimental plasma system. Steady-state argon plasma was generated using a linear plasma device, NAGDIS-II [13]. The electron temperature, electron density, and space potential measured using the Langmuir probe method were 3 eV,  $1.5 \text{ m}^{-3}$ , and  $-3 \text{ V}$ , respectively. To simulate the surface roughness of the machine marks on the initial ITER divertor surface, tungsten samples (The Nilaco Corp.) of size  $\sim 10 \text{ mm} \times \sim 10 \text{ mm} \times 0.2 \text{ mm}$  were scratched using sandpaper (#100) before insertion into the plasma. The tungsten samples were inserted into the plasma such that the surface was perpendicular to the magnetic field direction. The temperature of the specimens was measured using a radiation thermometer. The incident energy ( $E_i$ ) of the sample was varied by applying a sample bias.

Figure 4 shows a photograph of a sample without plasma irradiation (S0) and sputtered samples with varying  $E_i$  values (S1–S6). The sputtering conditions are listed

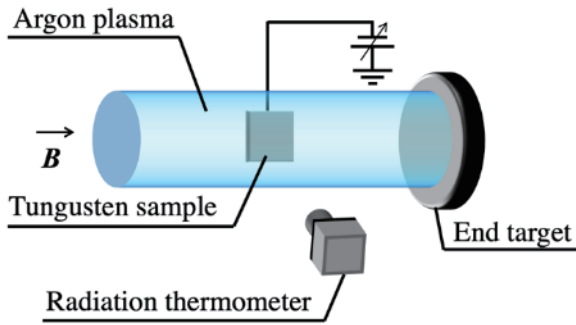


Fig. 3 Schematic of the sputtering experimental system.

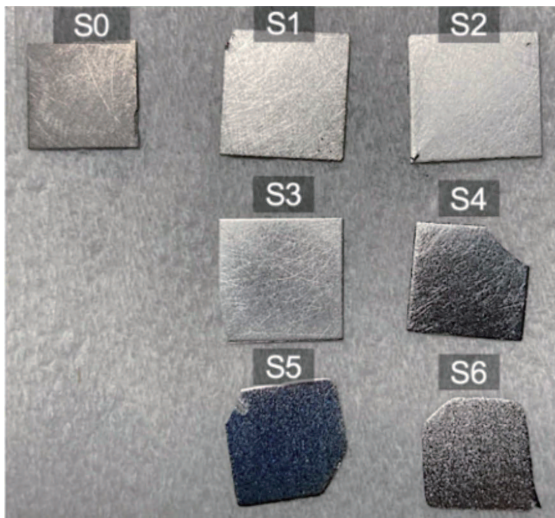


Fig. 4 Test samples.

Table 1 Sputtering conditions and surface roughness.

	$E_i$ [eV]	Specimen temp. [K]	Fluence [ $\times 10^{24} \text{ m}^{-2}$ ]	Sputtering yield [-]	$R_a$ [ $\mu\text{m}$ ]
S0	-	-	-	-	0.258
S1	40	990	8.1	$7.65 \times 10^{-4}$	0.226
S2	70	1117	9.4	$16.7 \times 10^{-3}$	0.180
S3	109	1236	10	0.101	0.122
S4	206	1419	11	0.286	0.115
S5	313	1538	13	0.415	0.0887
S6	409	1543	16	0.42	0.136

in Table 1. The incident ion energy, specimen temperature, fluence, and sputtering yield monotonically increased from S1 to S6. The surface of each sputtered sample was observed using a laser microscope (KEYENCE Corp.: VK-9700), as shown in Fig. 5. As  $E_i$  increased, scratches on the surface gradually disappeared. Scratches on S5 were difficult to observe; however, polygonal structures could be observed, and they were even larger in S6 than in S5.

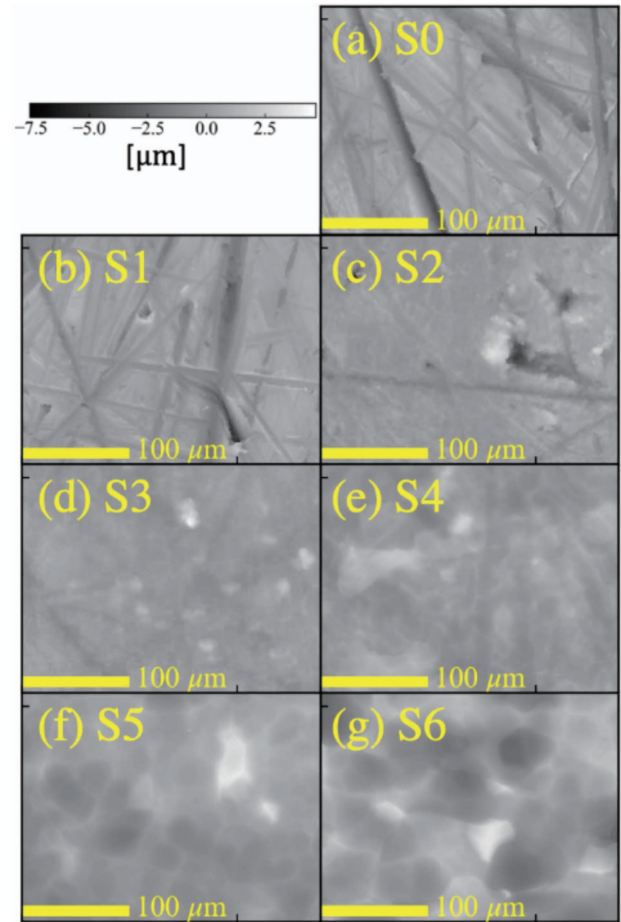


Fig. 5 Sample surfaces measured by the laser microscope.

The average surface roughness ( $R_a$ ) was obtained by averaging the surface roughness elements ( $r_a$ ) calculated within the range of moving square windows, whose one side was approximately 10 times longer than the wavelength of the laser. The window was moved both horizontally and vertically on the surface. The  $R_a$  is expressed as  $r_a = \langle |h - \mu_h| \rangle$ , where  $h$  denotes the height of the surface,  $\mu_h$  is the mean height,  $| \cdot |$  is the absolute operation, and  $\langle \cdot \rangle$  is the mean operation. The height was measured using a laser microscope. The initial  $R_a$  of the samples before sputtering was  $0.278 \mu\text{m}$  on average, and the  $R_a$  of S0–S6 are listed in Table 1.

#### 4. BRDF Measurement Results

Figures 6(a) and (b) show the BRDFs of the samples when s- and p-polarized light was incident on them at  $30^\circ$ , respectively. In both s- and p-polarizations, the peak of the BRDF of the sample increased with increasing  $E_i$  from S0 to S5, except for S1. Because the reflected light from S1 is anisotropic owing to the relatively large scratch on the surface, the peak value of S1 is an outlier. S6, which was sputtered with the largest  $E_i$ , had a BRDF smaller than S3–S5, which were sputtered with a smaller  $E_i$ . This is attributed to the  $R_a$  of S6 being larger than those of S3–S5,

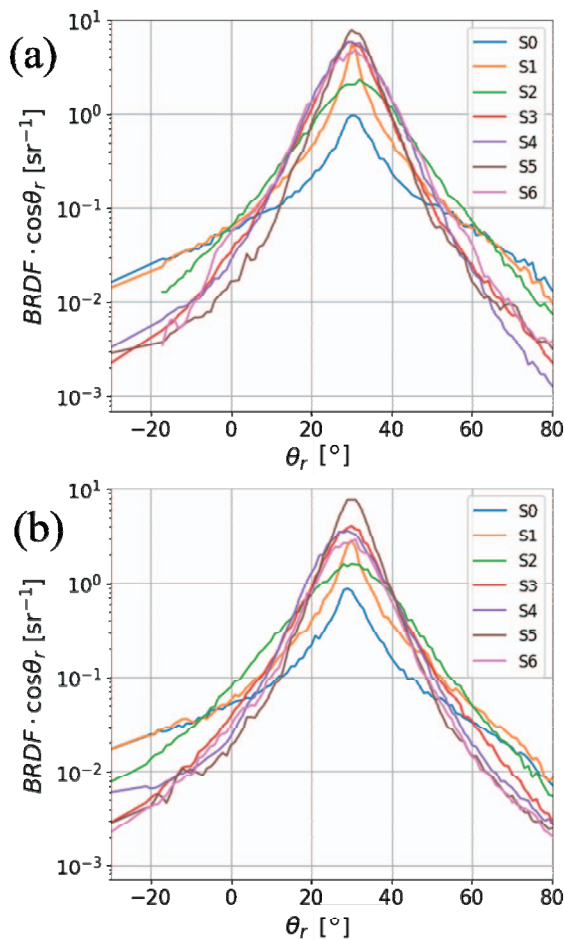


Fig. 6 BRDFs of sputtered samples with the incident (a) s- and (b) p-polarized light.

resulting in a larger spread of the reflected light.

In addition to the physical structure of the surface, ion irradiation can change optical constants [14]. The change in the optical constants varies the reflectance, resulting in a change in shape and the absolute value of the BRDF. When comparing the measured BRDFs in Fig. 6, the shape of the BRDF differs remarkably, which is attributed to the physical structure of the surface. Therefore, the peak values and full width at tenth maximum (FWTM) of the BRDFs of S2–6 with incident s- or p-polarized light and angles ranging from 15 to 60° are plotted as a function of  $R_a$  in Figs. 7 and 8, respectively. The peak values of all four incident angles increased linearly with increasing on a logarithmic scale, and there were several variances between the peak values of S2 and S5. The variances in the peak values between the incidence angles appeared according to Fresnel’s law and were particularly clear for s-polarized light. Because the reflectance of p-polarized light differed slightly in the range from  $-15^\circ$  to  $-60^\circ$ , it was difficult to determine the differences among incident angles in p-polarized light reflected from rough surfaces. Because the reflectance of p-polarized light is smaller than that of s-polarized light at a specific  $\theta_i$ , the p-polarized BRDF peaks

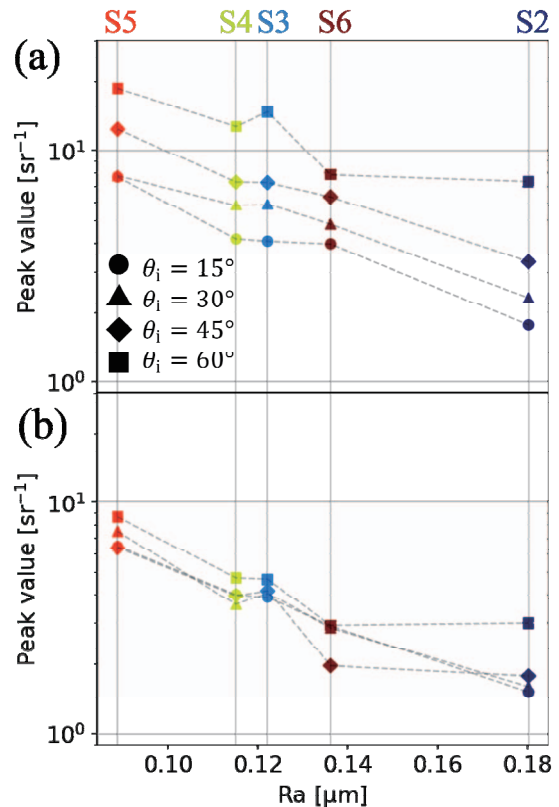


Fig. 7 Peak values of BRDFs with the incident (a) s- and (b) p-polarized light.

are also smaller than the p-polarized BRDF peaks at  $\theta_i$ . The FWTM decreased as  $R_a$  also decreased, resulting in the narrowing of the lobes of the reflected light. The difference between S2 and S5 in the FWTM was approximately two times. Additionally, there were slight differences in the FWTM depending on the angle of incidence and the polarized light direction.

### 5. Discussion

A scanning electron microscope (SEM) image of S6 is shown in Fig. 9. Polygonal structures were also observed on the surface. The specimen temperature during the sputtering of S6 was almost equal to the recrystallization temperature of tungsten. Consequently, recrystallized crystals likely grew, making the surface rougher. In addition, the peak value and FWTM scatter of S6 exhibit a similar trend to those of the scratched samples in Figs. 7 and 8. Although there were no mechanical scratches on S6, a different structure was formed on the surface by sputtering.

By considering only the sputtering and recrystallization effects, uneven structures on the surface, such as machine marks, can be removed through sputtering. A large  $E_i$  results in specular reflection, and the lobes of the reflected light becoming narrower. However, if the specimen temperature exceeds the recrystallization temperature, the surface becomes rough owing to the recrystallized crystals.

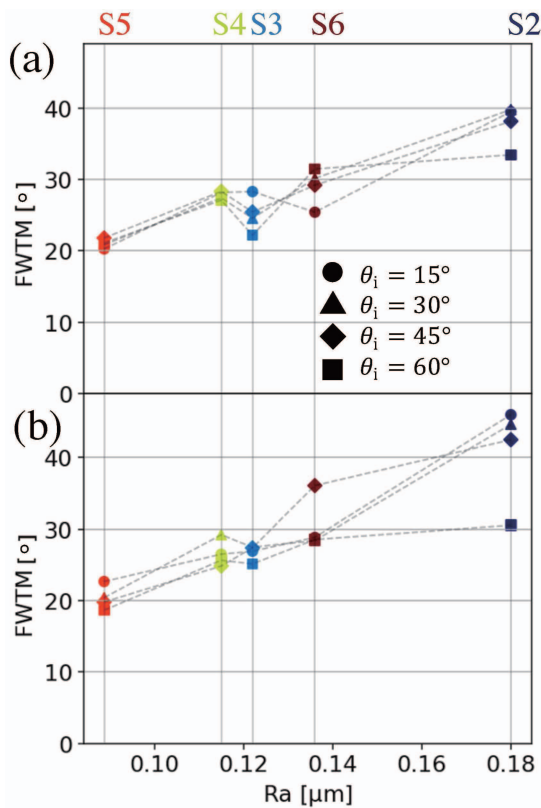


Fig. 8 FWTMs of BRDFs with incident (a) s- and (b) p-polarized light.

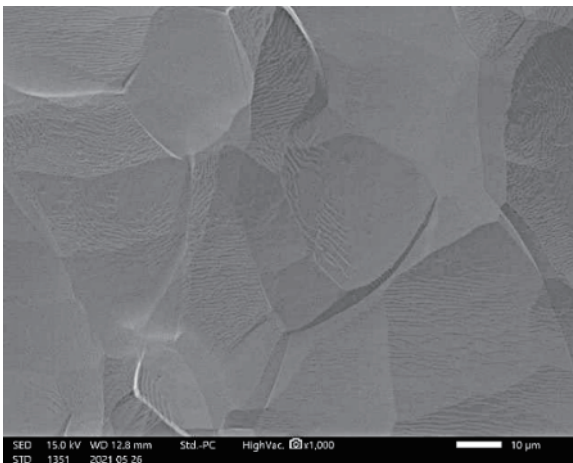


Fig. 9 Scanning electron microscope image of S6 with a magnification of 1,000.

The recrystallized crystals reduced the specular reflection and enlarged the diffuse reflection. Because the surface temperature of the baffles is expected to be lower than the recrystallization temperature [15], the specular reflection from the baffle region might have a significant effect on the spectroscopic measurements.

The wavelength dependence of the reflectance measured using a spectrophotometer (JASCO Corp., V-750) is shown in Fig. 10. The reflectance did not differ significantly

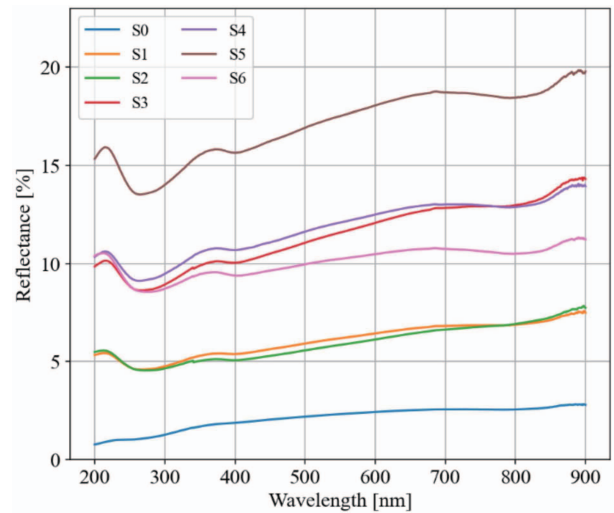


Fig. 10 Wavelength dependence of reflectance.

cantly among the samples and showed a similar trend in the measured wavelength range. According to [6], there is little change in the shape of the BRDF with wavelength, although the absolute value changes. If the ratio of  $R_a$  to  $\lambda$  is greater than unity, a ray is significantly occluded by an uneven structure on the surface [16]. However, because the present samples exhibited  $R_a/\lambda < 1$  with wavelengths over approximately 200 nm, it seems that there was little occlusion.

## 6. Summary

To understand the optical reflection characteristics corresponding to the surface condition of the divertor for accurate spectroscopic measurements, we constructed a goniophotometer and investigated the BRDF of tungsten samples sputtered in argon plasma generated by a linear plasma device. As the incident ion energy increased, the surface gradually smoothed such that the specular reflection became larger and the lobe of the reflected light became narrower. Near the recrystallization temperature, the recrystallized crystal likely makes the surface rough and the reflected light spread. Because the range of experimental conditions was limited in this study, for future work, further investigations with longer irradiation times are of interest.

## Acknowledgments

This work was partially supported by the DII Collaborative Graduate Program for Accelerating Innovation in Future Electronics at Nagoya University. One of the authors (H. N.) is grateful to the Naka Fusion Institution for hospitality and support during his internship in the second half of 2021.

[1] S. Kajita *et al.*, Plasma Phys. Control. Fusion **55**, 085020 (2013).

- [2] M. Carr *et al.*, Rev. Sci. Instrum. **90**, 043504 (2019).
- [3] S. Kajita *et al.*, Contrib. Plasma Phys. **56**, No. 9, 837 (2016).
- [4] V.S. Neverov *et al.*, Plasma Phys. Control. Fusion **62**, 115014 (2020).
- [5] H. Natsume *et al.*, Plasma Fusion Res. **16**, 2405019 (2021).
- [6] A. Iwamae *et al.*, JAEA-Research 2011-045 (2011).
- [7] P. Matia-Hernando *et al.*, Fusion Eng. Des. **158**, 111716 (2020).
- [8] M. Ben Yaala *et al.*, Rev. Sci. Instrum. **92**, 093501 (2021).
- [9] M. Yajima *et al.*, Plasma Sci. Technol. **15**, No.3, 282 (2013).
- [10] S. Kajita *et al.*, Nucl. Mater. Energy **25**, 100828 (2020).
- [11] R.L. Cook and K.E. Torrance, ACM Trans. Graphics **1**(1), 7 (1982).
- [12] Purdue University, *Thermophysical Properties of Matter; Vol. 7: Thermal Radiative Properties of Metals* (Plenum, New York, 1970).
- [13] N. Ohno, Plasma Phys. Control. Fusion **59**, 034007 (2017).
- [14] K. Ono *et al.*, J. Nucl. Mater. **463**, 952 (2015).
- [15] A. Khan *et al.*, Nucl. Mater. Energy **20**, 100674 (2019).
- [16] K.E. Torrance and E.M. Sparrow, J. Opt. Soc. Am. **57** (9), 1105 (1967).